Reflection/Diffraction Separation of Local Directional Projection Signals Using Implicit Neural Representations

Shustak Matan, Levy Ronit, Mandelman Elana and Koren Zvi*

Summary

Accurate seismic imaging of complex subsurface geology requires preserving both dominant specular reflections and low-amplitude, non-specular - diffraction - scattering energy associated with small-scale discontinuities such as fractures, channels, and cavities. Conventional migration workflows typically collapse angle-dependent information through stacking or averaging, which enhances specular energy but suppresses or destructively interferes with weak yet geologically critical signals. As a result, fine-scale features are often masked by high-amplitude reflections.

In this work, we present a novel method for robust decomposition of the total seismic scattering wavefield into specular (reflection) and non-specular (diffraction) components using Implicit Neural Representations (INR) applied to Local Directional Projection (LDP) signals generated within the Local Angle Domain (LAD) imaging framework (Koren and Ravve, 2011). The proposed approach exploits the fundamentally different directional and coherence characteristics of specular and non-specular events to achieve high-fidelity separation without relying on hard thresholds, directional smoothing, or explicit diffraction criteria.

Introduction

Local Directional Projection Representation

Within the LAD framework, recorded seismic events are back-projected to subsurface scattering points using simulated incident and scattered rays along a reference velocity model. At each image grid node, events are binned according to two pairs of spherical angles: directional dip and azimuth, and opening angle and azimuth, defined by the local ray geometry. This decomposition provides a natural separation between specular reflections - high-amplitude, directionally concentrated energy aligned with reflector normals - and non-specular events, which are lower in amplitude and distributed across a wider angular range.

For each subsurface point, the LAD output is reorganized into a set of Local Directional Projection (LDP) signals, where each signal represents a weighted average of events within a given directional bin across a finite spatial window spanning approximately one dominant wavelength. LDP signals can be generated directly during LAD migration or reconstructed from directional image gathers $D(\boldsymbol{x}, \boldsymbol{\nu})$ as

$$p(\boldsymbol{x}, \boldsymbol{\nu}, r) = D(\boldsymbol{x} + r\boldsymbol{n}(\boldsymbol{\nu}), \boldsymbol{\nu}) \quad for \quad r \in [-\frac{l}{2}, \frac{l}{2}], \tag{1}$$

where p is an LDP signal, $\boldsymbol{x} = (x, y, z)$ is a given subsurface scattering point, $\boldsymbol{n}$ is the directional unit vector at $\boldsymbol{x}$ associated with the spherical angle $\boldsymbol{\nu}$, and l is the radius length, estimated by the wavelength (Kletenik-Edelman et al., 2025). Transformation of these signals to the local wavenumber domain further enhances separation, where specular reflections manifest as compact, Gaussian-like beams.

Figure 1 illustrates the data preparation process. Starting with directional gathers (top), transforming to LDP around a given image point (middle) and applying the projection-slice theorem (1D Fourier transform over the LDP signals) to present the LDP in the local k-domain (bottom). The plotted k-domain LDP can be considered as 3D spherical sub-volumes illustrated in a 2D dip-radius view.

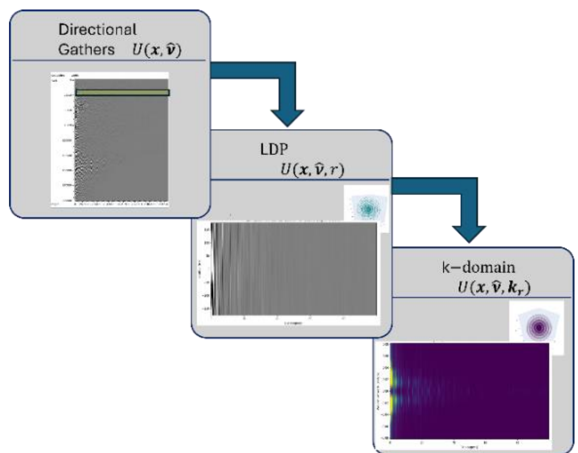

Figure 1: The data preparation process. The horizontal axis in all three plots are directional angles $\boldsymbol{\nu}$ – monotonously increasing dips with rotating azimuths – spiral representation. Starting with a group of directional gathers where the vertical axis is depth (top), transforming to LDP around a given image point – the vertical axis r is a distance from the central projected signal in the $\boldsymbol{\nu}$ direction (middle). The bottom plot is a result of application of the projection-slice theorem (1D Fourier transform over the LDP signals) where the LDP is presented in the local k-domain.

Although previous approaches using LDP specularity weights have shown promise (Kletenik-Edelman et al., 2025), their performance degrades in regions where specular and non-specular fields are strongly entangled. This motivates the use of a more expressive, continuous representation.

Reflection/Diffraction separation of LDP signals using INR approach

Method

INR-Based Specular Modeling

We employ an Implicit Neural Representation to model the specular component of the seismic wavefield in the LDP wavenumber domain. Rather than treating seismic data as discrete samples, the INR learns a continuous mapping from spatial and directional coordinates to seismic amplitude. A Sinusoidal Representation Network (SIREN) architecture (Sitzmann et al., 2020) is used, leveraging sinusoidal activation functions that are particularly well suited for oscillatory, band-limited seismic wavefields and mitigate spectral bias.

The network maps continuous subsurface coordinates to a set of physically meaningful specular parameters: peak wavenumber (k_0), reflector-normal direction ($\hat{\boldsymbol{k}}$), specular beam sharpness (σ_k), specular beam spread ($\sigma_\perp$), signal amplitude (A) and phase (ϕ). These parameters define a predicted 3D Gaussian beam specular model in k-space:

$$U_{pred}(\boldsymbol{k}) = A\ exp\left(\frac{(k_\parallel - k_0)^2}{2\sigma_k}\right) exp\left(\frac{k_\perp^2}{2\sigma_\perp}\right) e^{i\phi}\ , \tag{2}$$

where $k_\parallel = \boldsymbol{k} \cdot \hat{\boldsymbol{k}}$ and $k_\perp = \sqrt{\|\boldsymbol{k}\|^2 - k_\parallel^2}$,

representing the dominant specular energy at each image point. Due to their smoothness and directional coherence, specular reflections are efficiently captured by this compact representation. In contrast, incoherent, multi-directional, and low-amplitude scattering energy cannot be represented efficiently and is therefore excluded from the learned model.

Loss Function and Training

The network is optimized using a physics-informed **loss equation** that prioritizes magnitude-only comparison to account for k-domain phase sensitivity. The objective function is defined as:

$$\mathcal{L} = \left\| U\left(\boldsymbol{x}, k_0, \hat{\boldsymbol{k}}, \sigma_\perp, \sigma_\parallel, A, \phi\right) - U(\boldsymbol{x}, \boldsymbol{k}) \right\|^2 + \mathcal{L}_{reg}\ , \tag{3}$$

where $U\left(\boldsymbol{x}, k_0, \hat{\boldsymbol{k}}, \sigma_\perp, \sigma_\parallel, A, \phi\right)$ is the predicted specular local field of the observed LDP $U(\boldsymbol{x}, \boldsymbol{k})$ in the wavenumber domain, and $\mathcal{L}_{reg}$ represents a regularization penalty.

Specular–Non-Specular Separation

A key advantage of the proposed framework is that non-specular energy naturally emerges as a residual orthogonal to the learned specular field. After training, the inferred specular wavefield is adaptively removed from the observed data using projection-based subtraction in the wavenumber domain,

$$U_{res}(\boldsymbol{x}, \boldsymbol{k}) = U_{obs}(\boldsymbol{x}, \boldsymbol{k}) - \frac{\langle U_{obs}, U_{pred} \rangle}{\langle U_{pred}, U_{pred} \rangle} U_{pred}(\boldsymbol{x}, \boldsymbol{k})\ . \tag{4}$$

This suppresses high-energy reflections while preserving low-amplitude scattering signatures without contamination or leakage.

Figure 2 illustrates the basic INR architecture that encodes and predicts spatial functions of specular parameters. The high-resolution functions are used to predict and adaptively subtract the specular energy from the original, directionally decomposed, data.

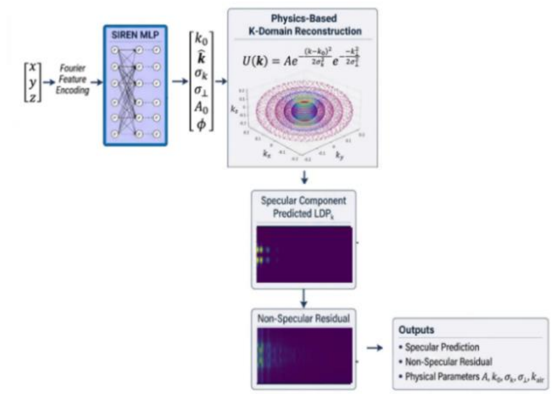

Figure 3 - Basic INR architecture that encodes and predicts spatial functions of specular parameters. The high-resolution functions are used to predict and adaptively subtract the specular energy from the original, directionally decomposed, data.

The resulting decomposition preserves the directional integrity of both components - the specular field retains accurate dip and azimuth information for structural interpretation, while the non-specular residual isolates subtle diffraction energy associated with fractures and other fine-scale geological features.

Field Data Example

The proposed method was applied to a land seismic survey acquired in the Eagle Ford Play of south-central Texas. The dataset covers approximately 130 square miles and is characterized by pronounced structural complexity, including intricate fault systems and a deep graben structure developed within alternating sequences of sand, silt, and clay.

To assess the preservation of low-amplitude, fine-scale geological discontinuities - such as fracture networks and small-offset faults - our analysis focuses on a target window of 100 inlines by 100 crosslines. The initial evaluation is performed using directional dip/azimuth gathers, which are fundamental for diagnosing the directional separation of the seismic wavefield.

Within these gathers, the total scattered wavefield is decomposed into its in-situ directional components at each image point. This representation enables clear discrimination between high-energy specular reflections, which appear as localized and coherent energy concentrations, and low-amplitude non-specular energy associated with subsurface diffractors. Examination of these gathers confirms that subtle scattering signatures remain isolated from the dominant reflections. This diagnostic step ensures that the subsequent INR-based parameterization accurately captures the specular field without inducing the destructive interference of underlying low-energy information that commonly arises from conventional migration averaging.

Figure 3 illustrates the resulting high-fidelity separation of the wavefield components for a representative directional gather, comparing the original input with the INR-inferred specular component and the corresponding non-specular residual. The results demonstrate the model's ability to accurately represent dominant specular energy using parametric Gaussian beams while successfully isolating low-amplitude scattering energy associated with fine-scale geological features.

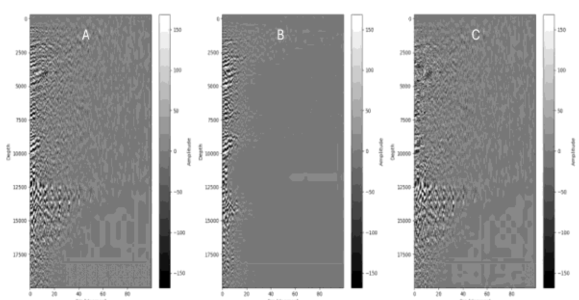

Figure 4 – Full Azimuth Directional gathers, original – full field (A) gather, INR-inferred specular field (B) and residual non-specular/diffracted Field (C)

To gain deeper insight into the wavefield modeled by the Implicit Neural Representation, we move beyond the analysis of discrete, point-wise gathers and examine the continuous parameter fields synthesized by the network. The adopted SIREN architecture enables a differentiable mapping from continuous spatial coordinates to a set of physically constrained specular attributes, including peak amplitude, central wavenumber, and reflector-normal direction.

A critical diagnostic step in this framework is assessing whether these parametric fields accurately follow the underlying specular structure, and geological trends present in the original seismic data. Figure 4 illustrates this evaluation through a depth slice at 14,260 ft within the Eagle Ford volume. At this depth, a prominent high-angle fault is observed cutting across the primary reflection surfaces. Importantly, the spatial distribution of the inferred specular parameters exhibits strong correspondence with the reflectivity image, closely tracking the geometry and continuity of the fault system.

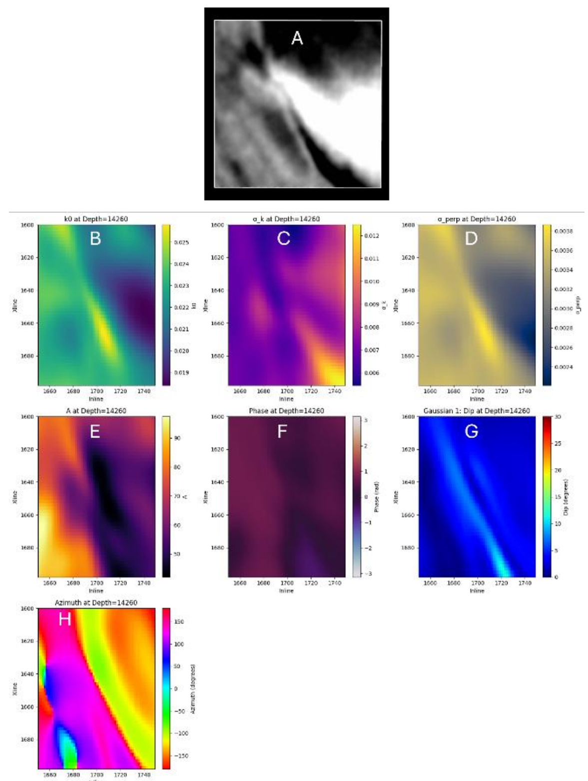

Figure 5 – INR-Inferred specular parameters. The seismic image (A), central wavenumber (B), beam sharpness (C), beam spread (D), Amplitude (E), phase (F), beam dip angle (G) and beam azimuth (H).

This high degree of alignment demonstrates that the network's continuous parameter field accurately captures the dominant specular reflections and their associated structural features. As a result, the high-energy reflection components are effectively absorbed into the learned specular model, ensuring that the low-amplitude, non-specular residual remains isolated and preserved for subsequent analysis and characterization of fine-scale geological features.

Following validation of the continuous parameter fields, we assess the fidelity of the wavefield separation to ensure that removal of the dominant reflections does not compromise the integrity of the underlying scattered wavefield. Using projection-based subtraction, the high-amplitude specular component is orthogonally removed, thereby protecting low-energy scattering information that is typically degraded or lost due to the destructive interference inherent in conventional migration averaging.

Figure 5 presents a depth slice at 11,620 ft within the volume, where a complex fault system is largely obscured by dominant, high-amplitude specular reflections in the original stacked image. After removal of the inferred specular energy through the INR-based decomposition, these structural discontinuities and associated small-scale features become clearly discernible. A comparative analysis of the original stack, the synthesized specular model, and the resulting non-specular residual confirms that intricate geological details - including fracture systems and small-offset faults - are effectively isolated and preserved within the residual wavefield.

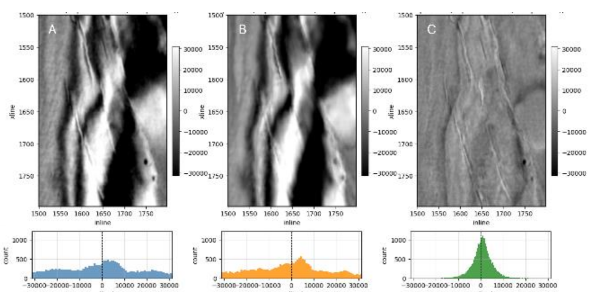

Figure 6 - Depth section at 11620ft. a comparison between the original image (A), the INR-inferred specular image (B) and the non-specular image (C). The corresponding histograms below indicate the number of events with respect to the amplitude values. The three histograms below indicate the corresponding contribution number of each amplitude bin.

The application of the proposed method to the Eagle Ford Play dataset demonstrates its capability to characterize complex subsurface structures, including intricate fault systems and a deep graben. By analyzing a targeted 100x100 line window, we confirmed that the INR-SIREN architecture successfully learns a continuous field of physically constrained specular attributes - such as peak amplitude, central wavenumber, and reflector-normal direction - that align precisely with prominent geological trends. The depth section at 11,620 ft (Figure 5) highlights the method's primary advantage: the removal of dominant, high-energy specular reflections reveals subtle, small-scale features that were previously obscured. A comparative analysis confirms that orthogonal residual extraction meticulously isolates and preserves the low-amplitude non-specular scattering wavefield, ensuring that fracture systems and small-offset faults are maintained with high fidelity rather than being destroyed by conventional migration averaging.

Conclusions

We have developed a robust automatic method for reliably extracting the specular components of the seismic scattering field while preserving the low-amplitude, non-specular scattering events. The LDP signals provided by the LAD imaging system is a key step in this method. Applying Implicit Neural Representations (INR) with the SIREN architecture, in the wavenumber (k-domain), we achieve a high-fidelity separation that overcomes the resolution loss inherent in traditional migration algorithms. The resulting continuous parameter fields - modeling specular energy as 3D Gaussian beams - provide physically meaningful structural attributes, including high-resolution dip and azimuth maps. This methodology ensures that fine-scale geological discontinuities, such as fracture networks, are captured and protected within the non-specular residual. Ultimately, these rich physical attributes provide a superior foundation for automated AI-based interpretation and advanced reservoir characterization.

Refrences

Kletenik-Edelman, O., Zaslavsky, A., Shustak, M., Levy, R. and Koren, Z., 2025, Local Directional Projection (LDP) specularity weights for enhancing and characterizing seismic reflectivity images, Extended Abstract, IMAGE 2025 – International Meeting for Applied Geoscience & Energy, Houston

Koren, Z., and Ravve, I., 2011, Full-azimuth subsurface angle domain wavefield decomposition and imaging, Geophysics.

Sitzmann, V., Martel, J., Bergman, A., Lindell, D., and Wetzstein, G., 2020, Implicit neural representations with periodic activation functions. Advances in neural information processing systems, 33:7462–7473, 2020.